Investigating Water Electrolysis for Efficient Oxygen Production in Microgravity

Sanjay Karthik[1] and Aidan Sherin[2]
University of Florida, Gainesville, Florida, 32611, United States of America

Sunjae Kim[3]
University of Florida, Gainesville, Florida, 32611, United States of America

Abstract

Currently, the total power consumption for oxygen generation in NASA's crewed missions is 1.5 kW, which is about one third of the total life support system power. The water electrolysis reaction is leveraged to produce needed oxygen gas for NASA's crewed missions. Yet, future exploration missions to Mars will require oxygen generation systems that are both more compact and power efficient. A key research need is to quantify how reduced and partial gravity affects water electrolysis performance and to identify approaches that maintain high efficiency in these environments. Under reduced buoyancy, oxygen and hydrogen bubbles generated at the electrodes do not detach readily and can remain attached near their nucleation sites, which restricts electrolyte replenishment and reduces the effective reactive surface area. Consequently, sustained bubble coverage can form an insulating gas layer that increases interfacial resistance, elevates ohmic losses and overpotential, and ultimately degrades electrolysis efficiency. This study investigates bubble detachment behavior and electrolysis performance under both terrestrial and simulated microgravity conditions using Computational Fluid Dynamics analysis in Ansys Fluent. A Volume of Fluid multiphase model is employed to capture gas-liquid interface dynamics, with results validated against terrestrial experimental data obtained through Linear Sweep Voltammetry of the Oxygen Evolution Reaction. A mesh independence study was conducted to optimize simulation accuracy and computational efficiency. The validated 1G Computational Fluid Dynamics model is then extended to a zero-gravity environment to characterize the degradation in bubble detachment and electrolysis efficiency under microgravity conditions. This work establishes a validated computational framework for evaluating electrolysis performance in reduced gravity directly supporting the development of future NASA In Situ Resource Utilization architectures and Environmental Control and Life Support System technologies.

I. Nomenclature

μG	=	microgravity
j	=	current density
V	=	applied cell voltage
μm	=	micrometers ($1x10^{-6}$ m)
F_{qs}	=	Quasi-steady Drag Force
F_{du}	=	Unsteady Growth Force

[1] Undergraduate Research Assistant, KIMSLAB, Department of Mechanical and Aerospace Engineering, AIAA Member (1763024) Undergraduate Freshman, *sanjay.karthik@ufl.edu*
[2] Undergraduate Research Assistant, KIMSLAB, Department of Mechanical and Aerospace Engineering, AIAA Member (1900596) Undergraduate Freshman, *asherin@ufl.edu*
[3] Assistant Professor and Principle Investigator of KIMSLAB, Department of Mechanical and Aerospace Engineering, AIAA Member, *sunjae.kim1@ufl.edu*

F_{sL} = Shear Lift Force
F_B = Buoyancy Force
F_{st} = Surface Tension Force
F_h = Hydrodynamic Pressure Force
F_{cp} = Contact Pressure Force

II. Introduction

Long-duration human spaceflight demands reliable, onboard oxygen generation systems capable of operating efficiently in reduced-gravity environments. Water electrolysis, the electrochemical splitting of water into hydrogen and oxygen, is a cornerstone technology for NASA's Environmental Control and Life Support System (ECLSS) aboard the Human Landing System (HLS). However, the absence of buoyancy-driven convection in microgravity fundamentally disrupts this process. Without gravity to detach and transport gas bubbles from electrode surfaces, O_2 and H_2 bubbles accumulate at the cathode and anode respectively, blocking active reaction sites, increasing ohmic overpotential, and reducing electrolysis efficiency by an estimated 30–40% compared to terrestrial performance [9]. Solutions such as forced convection and propellant management devices (PMDs) introduce mass, volume, and mechanical complexity that are difficult to justify for ECLSS integration.

This experiment investigates electrolysis vapor nucleation for microgravity environments. Microgravity conditions are simulated through computational fluid dynamics (CFD) analysis using ANSYS Fluent. The simulation employs a Volume of Fluid (VOF) multiphase model to capture gas-liquid interface dynamics in a zero-gravity environment. Results are validated against published literature as well as this study's 1G test cases to establish confidence in the model before parametric studies are conducted. This work aims to provide proof of the need for a system of bubble detachment to replace buoyancy force for future integration into NASA ECLSS electrolyzers.

III. Background Theory

A. Bubble Theory

In the reaction of electrolysis, vapor bubbles are generated electrochemically at the electrode surface rather than thermally. Despite this difference in origin, the hydrodynamic forces governing bubble departure and lift-off remain the same. A nucleating bubble on the electrode surface experience forces in two directions: parallel to the surface and normal to it. The dominant forces are quasi-steady force (F_{qs}), unsteady growth force (F_{du}), shear life (F_{sL}), buoyancy (F_B), surface tension (F_{st}), and pressure forces (F_h, F_{cp}) [3, 4]. Surface tension anchors the bubble to the electrode until the contact diameter diminishes sufficiently at departure. Quasi-steady drag, driven by relative velocity between the bubble and surrounding liquid, typically exceeds surface tension by 2-3x and is the primary force promoting bubble sliding [4]. The growth force arises from asymmetric bubble expansion and produces components both opposing drag and pressing the bubble toward the surface. Buoyancy, resulting from the density difference between the gas bubble and liquid, drives lift-off in the wall-normal direction. Shear-lift, generated by the velocity gradient near the electrode surface, creates an additional transverse force through induced vorticity within the bubble [5]. At lift-off, F_{st}, F_{cp}, F_h are all become negligible as the contact diameter approaches zero, reducing the departure condition to $F_B + F_{du} = 0$ [3]. Understanding this force balance allows prediction of bubble departure and detachment frequency, both of which directly impact gas separation efficiency within electrolysis.

B. The Reaction of Electrolysis

Water electrolysis splits water into hydrogen and oxygen by applying an electrical potential across two electrodes in an electrolyte, with the reaction governed by interfacial phenomena in the three-phase zone where electrode, electrolyte and evolving gas bubbles meet [6]. Under terrestrial conditions, buoyancy drives bubbles off the electrode surface, but in microgravity, this force is essentially absent, causing bubbles to accumulate into a froth layer that increases ohmic resistance, blocks nucleation sites, and reduces mass transfer – all of which degrade system efficiency [7]. Electrode wettability is therefore critical. Water electrolysis is already central to space operations – the ISS

Oxygen Generation Assembly uses a PEM electrolyzer within the ECLSS to produce oxygen for life support – though gas bubble management within such systems remains an open engineering challenge in microgravity [7]

IV. Methodology & Design Process

A. Computer Aided Design (CAD) Model

The experimental apparatus was designed using SolidWorks as a fully assembled CAD model prior to fabrication. The structural frame consists of T-slot aluminum extrusion members joined together by gusset brackets, forming the cubic enclosure shown in Fig 1. This framing approach was meant to fit in the strict dimension constraints of 12”x12”x12”. It also allows for internal component repositioning. To be adjusted between test iterations without redesigning the entire structure. The side panels are modeled as flat transparent sheets, representative of the ABS plastic filament used in the physical build. Mounted to the bottom plate, is the electrolysis setup The electrolysis setup is situated directly on the base; each electrode is shown, where the generated gas bubbles are produced. The assembly captures the complete experimental configuration used to study the bubble separation behavior, and was used as the basis for dimensional verification and component fit check prior to physical fabrication

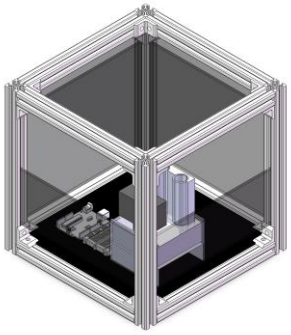

Figure 1: Experimental Test Setup CAD Model

C. Electrolysis & Circuit and Logic

This investigation requires the use of a circuit that serves as a medium for electric charges to travel through the electrolysis apparatus. As discussed, the characteristics of the circuit will be important in observing the relationship between voltage, current, and bubble production. Voltage and current produced by the 9V battery will need to be measured to determine the presence of overpotential and ohmic losses during bubble production. As a result, voltage and current sensors have been included in the circuit in parallel and series respectively. Specifically, voltage is considered an independent variable in the experiment to determine the relationship of current flowing under differing voltage outputs. A DC-DC buck converter will be utilized to decrease the amount of voltage entering the electrolysis setup with respect to the cell voltage. Another component in the circuit series is a MOSFET. This enables the circuit to be turned on and off with a microcontroller, proving beneficial in cases in which the apparatus would be inaccessible to the investigator, such as when conducting a drop tower experiment. The logic behind the MOSFET and data collection of current and voltage is done through an Arduino Uno microcontroller. The analog pins allow for data to be collected and interpreted within the IDE through an analog signal at a 9600 baud rate. Finally, the electrolysis setup will act as a resistor, being connected in series to the rest of the circuit. This resistance arises from the bubble nucleation.

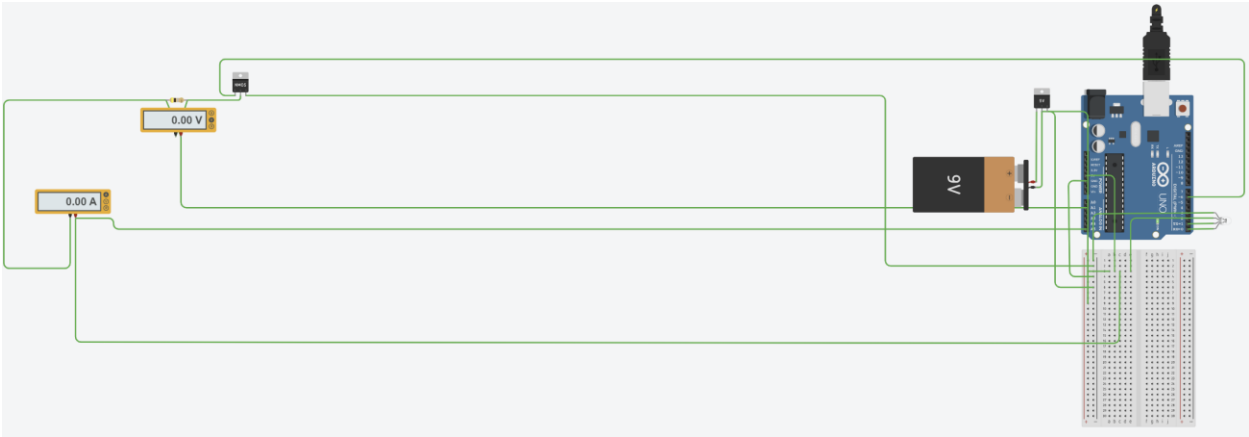

Figure 2: Electrolysis Circuitry

Beyond the physical circuit, the logic behind the collection of data is done within the Arduino IDE. The code defines constant variables depending on which pins are being utilized for data collection. Furthermore, calibration facilitates matching the values the program outputs to the real-world values. The code used for Arduino IDE was developed with the assistance of ChatGPT. To verify the sensor values produced, the DC-DC buck converter voltage value was compared, which showed a differing potential difference of 0.3V. This code is shown in appendix A.

D. **Computational Fluid Dynamics**

Computational Fluid Dynamics will be used in this investigation to run a transient simulation and validate the 1G case while also conducting μG with and without ultrasonic penetration of the fluid domain. The Volume of Fluid model (VOF) in 2D will create an interface between the oxygen gas and water liquid. This continuous-continuous interface ensures that both phases do not mix, providing sharper visualization for bubble behavior. The VOF model handles bubble behavior by solving mass and momentum equations at each cell. This is multiplied by a volume fraction. The volume fraction depicts the fraction of the cell that is in the liquid regime vs. gaseous regime. The former will be H_2O and the latter O_2. Table one depicts properties of these materials that are important for the VOF solver.

Fluid	Density, ρ	Viscosity, μ
H_2O	$998.20\ \frac{kg}{m^3}$	$1 \times 10^{-4}\ \frac{kg}{ms}$
O_2	$1.30\ \frac{kg}{m^3}$	$1.92 \times 10^{-5}\ \frac{kg}{ms}$

Table 1: Fluid Properties

Due to the inability for pressure to be solved in the momentum equations that VOF leverages, pressure-velocity coupling is used to infer and reiterate with equations to best predict the pressure of the fluid domain. In this simulation, the PISO method is used due to a transient case being run.

To create the cells required for VOF to solve the equation, a mesh needs to be formed on the surface of the geometry; however, there is a correct amount required to both satisfy efficiency and accuracy [2]. To satisfy this amount, a mesh

independence study was conducted. Three meshes were created and solved for five seconds total runtime with a velocity inlet and pressure outlet to simulate the 1G scenario. Table two depicts the results.

Mesh Level	Cell Count	Mass Produced
Coarse	44352	1.14 x 10^{-10} kg
Medium	72000	8.39 x 10^{-11} kg
Fine	121761	8.24 x 10^{-11} kg

Table 2: Mesh Independence Study Results

After determining the amount of error between the three mesh levels, the error present in the coarse to medium was 0.26% while the error present in the medium to fine mesh was only 0,01%. As a result, the medium mesh level will be adopted due to its near identical accuracy as the higher mesh count with more efficiency.

To simulate bubble nucleation along the electrode, a velocity inlet was created along a wall as a boundary condition. A pressure outlet was also created along the opposite wall to satisfy the conservation of mass. To determine the rate at which oxygen bubbles will be produced, Faraday's law of electrolysis can be used. This law states:

$$\dot{m} = \frac{\boldsymbol{Im}}{\boldsymbol{zF}}$$

Where mass flow rate ($\dot{m}$) is proportional to current (I) and molar mass (m) of oxygen (0.032kg/mol) while being inversely proportional to Faraday's constant (F) (96485C/mol). To procure the number of electrons transferred being four, it can be recognized through the oxygen half reaction for electrolysis:

$$2H_2O > O_2 + 4H^+ + 4e^-$$

When applying the following variables:

I = 1.47A
m = 0.032kg/mol
z = 4
F = 96485C/mol

$$\dot{m} = \mathbf{1.22 \times 10^{-7}\ kg/s}$$

For the purposes of satisfying the velocity inlet boundary condition, the mass flow rate can be converted with the following equations:

$$v = \rho\, \dot{m}\, \boldsymbol{A}$$

$$\rho = 1.429 \frac{kg}{m^3}$$

$$A = 0.0025\, \pi^2\, m^2$$

Where the velocity is proportional to the mass flow rate ($\dot{m}$)**,** fluid density **(**ρ) and the cross-sectional area of the inlet (A). Therefore, velocity is:

$$v = 3.46 \times 10^{-6}\, m/s$$

E. Experimental Variables

Variable Type	Variable Name	Parameters
Independent	**Potential Difference across Electrolysis Apparatus**	**0V – 7.21V**
Independent	**Gravitational Force**	**1G case for the experimental setup & 1G / µG CFD setup**
Dependent	**Current across Circuit**	**Calculated based on ammeter data in series of the circuit**
Control	**Electrolyte**	**A sodium sulfate solution (1.5M) was used**
Control	**Global Courant Number (CFD)**	**0.5 for adaptive time stepping**

Table 3: Experimental Variables

V. Results & Data Analysis

A. 1G Electrolysis Experiment

The Liner Sweep Voltammetry (LSV) curve, shown in Fig. 3, obtained for the Oxygen Evolution Reaction (OER) under terrestrial conditions reveals a characteristic current-voltage relationship that demonstrates the critical role of buoyancy force in maintaining electrolysis efficiency. The theoretical decomposition voltage for water is 1.23 V [10]. However, the onset of appreciable current only occurs at a higher applied voltage, the difference represents the total system overpotential. Ohmic overpotential is directly influenced by bubble accumulation on the electrode surface. The observable scatter in the data is consistent with transient bubble formation and detachment. The formation briefly disrupts the electrode-electrolyte solution contact and locally increases interfacial resistance. Under terrestrial conditions, buoyancy continuously acts opposite to the direction of gravity and detaches the accumulating vapor bubbles from the respective anode and cathode, replenishing the electrolyte's active nucleation site and limits sustained bubble coverage. In a microgravity environment, the absence of this buoyancy-driven detachment mechanism allows bubbles to rest around the electrode, progressively increasing ohmic overpotential and shifting the I-V curve rightward. This means there must be a higher voltage applied to achieve the same current density. This directly degrades the power efficiency of the electrolyzer.

Figure 4 provides a visual corroboration of the reaction captured in the LSV curve, illustrating the electrode surface and vapor/fluid response across five discrete operating conditions. At 1.22V and 0.43A, near the thermodynamic decomposition threshold, the electrode surface does not produce any visual bubble nucleation, consistent with operational documentation. As voltage increases to 2.9V and 0.77A, sparse discrete bubbles begin to appear and detach from the electrode surface, driven by buoyancy in the wall-normal direction. The transition to 5.80V and 1.33A marks a qualitatively distinct change of flow regime: vigorous bubble generation is evident, with significant vapor/fluid agitation and what appears to be froth layers developing at the top of the electrode. A direct manifestation of sustained bubble coverage increasing ohmic resistance at higher production rates, this would skyrocket the necessary applied voltage if not for Earth's gravitational force. Notably, at 6.30V the current marginally decreased to 1.30A despite increases applied voltage, which is consistent with momentary bubble accumulation on the anode surface elevating the interfacial resistance and suppressing current – a transient efficiency loss directly related to the degradation expected in microgravity. At 7.36V and 1.46A, the high driving potential overcomes this resistance, restoring and increasing current. This sequence visually demonstrates that even under terrestrial conditions with

buoyancy present, the electrode bubble coverage can temporarily degrade performance. This underscores the severity of the problem in a microgravity environment with where no buoyancy-driven clearing mechanisms exist.

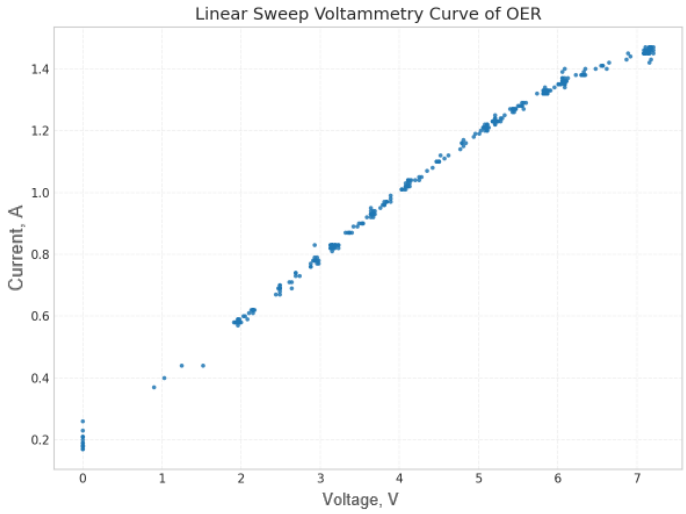

Figure 3: Linear Sweep Voltammetry Graph

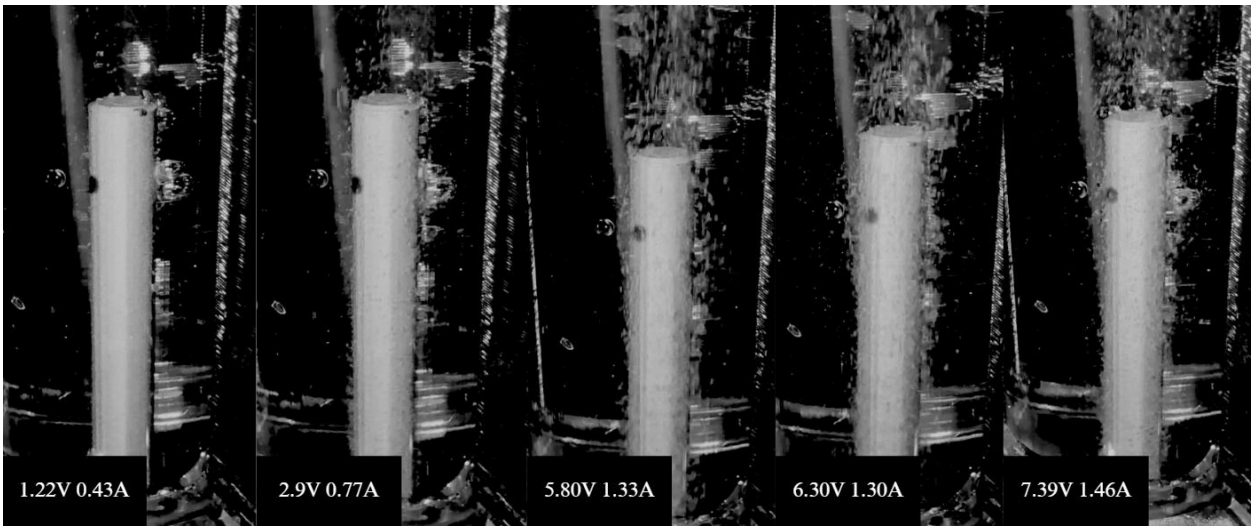

Figure 4: Visualization of the Anode During Electrolysis Reaction in 1G

B. CFD Result & Validation

The VOF simulation ran for 5s in 1G conditions under a bubble velocity representing that of the maximum bubble velocity for the experimental setup. Note that the x-axis is the axis of gravitational force. Correlating simulation to reality, the velocity inlet would be equivalent to a singular activation site of the OER along the electrode. This is an advantage of the simulation over experimentation. Analyzing a singular site versus the entire electrode means more focused analysis can facilitate without external factors. Though only simulating a singular site means that bubble behavior such as coalescence cannot be observed. This can affect the overall overpotential and ohmic loss observed in electrolysis. Bubble formation and departure are present. Due to buoyancy force opposing gravitational force, the bubbles rose from the velocity inlet towards the opposing pressure outlet. The contour graph in Fig. 5 indicates that there are distinct regions of a volume fraction of 0.5, which is the fraction depicting the boundary between gas and liquid. These are present for a limited time along the activation area before departing at a consistent rate to make room for a concurrent electrolysis reaction to occur. The iso-surface in Fig. 7 more clearly visualizes the shape and trajectory of bubbles as they escape from the electrode, proving the same behavior as the experimental setup. The

volume fraction indicates the ratio of liquid and gas in a singular mesh cell. When transitioning to a μG case, Fig. 6 shows that the oxygen bubbles clump along the activation site due to a lack of buoyancy force, which stems from a lack of gravitational force to oppose. This clumping caused the diffusion boundary layer along the activation site to increase, reducing bubble transport and overall OER as a result. This would induce increased ohmic losses and overpotential due to the reduction of activation sites for bubbles to depart from. To validate this CFD μG case, future experimentation through a drop tower would need to be conducted. Additionally, a bubble coalescence model should be included to further improve the observation of overpotential and ohmic loss. Nevertheless, through ensuring that the simulation was setup to provide increased accuracy through a mesh independence test and implementing a global courant number, it can serve to accompany the experimental case to provide qualitative bubble behavior data.

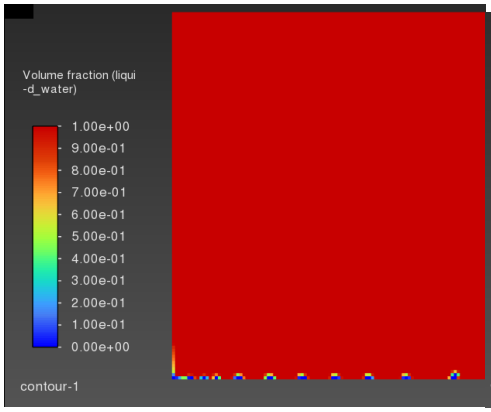

Figure 5: Contour Volume Fraction Graph 1G

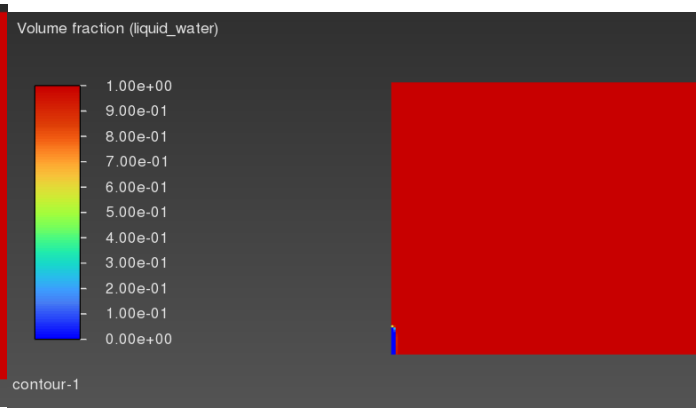

Figure 6: Contour Volume Fraction Graph *μG*

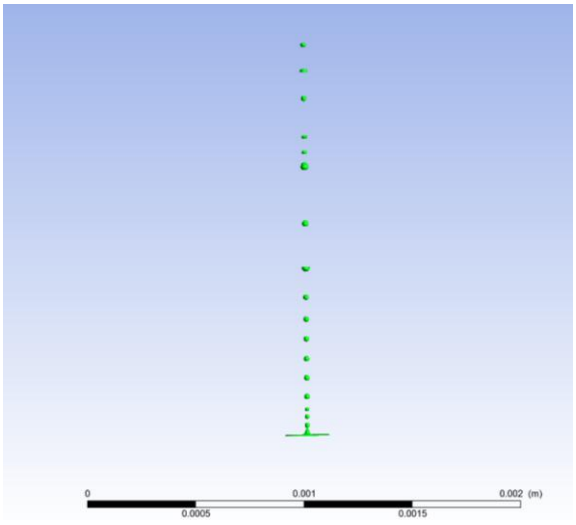

Figure 7: Iso-Surface Graph 1G

VI. Conclusion

The results of this investigation carry direct implications for the design and operational efficiency of NASA's Environmental Control and Life Support System, specifically the Oxygen Generation Assembly aboard the Human Landing System (HLS) and future crewed Mars transit vehicles. The LSV data in Fig. 3 and corresponding visual evidence from Fig. 4 demonstrate that even under terrestrial conditions, sustained bubble coverage at the anode surface introduces measurable ohmic overpotential that suppresses current density at a given applied voltage. Furthermore, the CFD simulation validates the qualitative experimental data regarding bubble behavior. Through a mesh independence study and observation of the global courant number, the data presented by the CFD solutions of the continuity and momentum equations are solved accurately. The simulation concludes that buoyancy force contributes to bubble departure in a 1G case and the lack of it causes clumping of oxygen along the activation site through qualitative data. This result would introduce increased ohmic loss and overpotential as a result. This CFD case introduces a foundation to create future investigations from, including acoustic immersion of electrolysis. In the microgravity environment of an operational ECLSS electrolyzer, where buoyancy-driven detachment is effectively absent, this bubble accumulation becomes a persistent rather than transient phenomenon, continuously degrading the reactive surface areas and driving up the voltage required to maintain the oxygen production rates necessary for crew life support. The ECLSS currently consumes approximately 1.5 kW for oxygen generation, representing roughly one third of the total life support power budget [9]. Any increase in ohmic overpotential due to unmanaged bubble coverage directly inflates this power demand. The acoustic forcing strategy proposed offers a compelling mitigation strategy; by promoting bubble detachment independent of gravitational acceleration, ultrasonic transducers could maintain electrode surface wettability and limit resistive losses to near-terrestrial levels without introducing the mechanical complexity or failure modes associated with rotating separators or forced convection systems currently employed in the ECLSS. Successful implementation of this approach could therefore reduce the electrolyzer power consumption of future deep-space life support systems.

Future work will focus on experimental validation of the microgravity CFD model through a drop tower experiment, following the same validation methodology applied to the terrestrial, 1G, case in this investigation. While acoustic forcing has demonstrated the ability to promote bubble detachment from the electrode's surface, the post-detachment trajectory is uncontrollable. In practical ECLSS implementation, unguided bubble transport through transfer lines and manifolds introduces the risk of hydrodynamic cavitation, which can degrade system performance and compromise hardware. To address this, a proposed next phase of development involves integrating the acoustic-electrolysis assembly within Propellant Management Device architecture, leveraging capillary and wetting forces to passively govern post-detachment bubble migration toward designated gas collection outlets. This coupled PMD-acoustic approach would provide end-to-end bubble management. This would offer a fully passive, gravity-independent oxygen generation strategy suitable for integration into NASA ECLSS electrolyzers.

VII. Appendix

```
// --- PIN DEFINITIONS ---
const int mosfetGate = 6;    // MOSFET Gate on Digital 6
const int voltmeterPin = A1; // Voltmeter on Analog 1
const int ammeterPin = A5;   // Ammeter on Analog 5

// --- CALIBRATION ---
float vDivider = 5.0;  // Set to 5.0 if using a 0-25V Voltage Sensor module
float aSens = 0.185;   // Sensitivity (0.185 for 5A, 0.100 for 20A, 0.066 for 30A)
float aOffset = 0;   // Voltage at 0 Amps (usually half of VCC)

// Timing for display
unsigned long previousMillis = 0;
const long interval = 500;

void setup() {
  pinMode(mosfetGate, OUTPUT);
  digitalWrite(mosfetGate, LOW); // Default to OFF for safety

  Serial.begin(9600);
  Serial.println("--- System Online ---");
  Serial.println("Pins: Gate(6), Volts(A1), Amps(A5)");
  Serial.println("Commands: 'ON' to start, 'OFF' to stop.");
}
```

```
void loop() {
  // 1. LISTEN FOR SERIAL COMMANDS
  if (Serial.available() > 0) {
    String command = Serial.readStringUntil('\n');
    command.trim();

    if (command.equalsIgnoreCase("ON")) {
      digitalWrite(mosfetGate, HIGH);
      Serial.println(">> MOSFET: ACTIVE");
    }
    else if (command.equalsIgnoreCase("OFF")) {
      digitalWrite(mosfetGate, LOW);
      Serial.println(">> MOSFET: INACTIVE");
    }
  }

  // 2. DATA PROCESSING & DISPLAY
  unsigned long currentMillis = millis();
  if (currentMillis - previousMillis >= interval) {
    previousMillis = currentMillis;

    // Voltage Calculation
    int rawV = analogRead(voltmeterPin);
    float voltage = (rawV * 5.0 / 1023.0) * vDivider;

    // Current Calculation (Averaged to reduce jitter)
    long rawSum = 0;
    for(int i=0; i<10; i++) { rawSum += analogRead(ammeterPin); }
    float avgRawA = rawSum / 10.0;
    float current = ((avgRawA * 5.0 / 1023.0) - aOffset) / aSens;

    // Display Output
    Serial.print("VOLTAGE: ");
    Serial.print(voltage, 2);
    Serial.print("V | CURRENT: ");
    Serial.print(current, 2);
    Serial.println("A");
  }
}
```

Code generated by ChatGPT on 2/26/2026.

VIII. Acknowledgments

The authors thank Dr. Sunjae Kim for his guidance, mentorship, and laboratory support throughout this research. The authors would also like to thank PHD student Dominic Meler for aiding us in the design process for the electrolysis circuit, bubble theory, and part logistics. The authors would also like to thank Yusin Jeong for his mentorship throughout the CFD setup, simulation, and post-processing flow. This work was conducted in the Kim Space Lab at the University of Florida. ChatGPT AI (OpenAI) was used to aid in the Arduino code writing process.

References

[1] (2026). Youtu.be. https://youtu.be/6BJauDTpCmo?si=pl7Dqr0nBoEEUkFM

[2] Wu, Z., Li, K., Han, W. *et al.* Simulation Analysis of Liquid Flow in a Vane-type Surface Tension Tank. *Microgravity Sci. Technol.* **34**, 80 (2022). https://doi.org/10.1007/s12217-022-09991-y

[3] Zeng, L. Z., Klausner, J. F., Bernhard, D. M., & Mei, R. (1993). A unified model for the prediction of bubble detachment diameters in boiling systems—II. Flow boiling. *International Journal of Heat and Mass Transfer*, *36*(9), 2271–2279. https://doi.org/10.1016/S0017-9310(05)80112-7

[4] Klausner, J. F., Mei, R., Bernhard, D. M., & Zeng, L. Z. (1993). Vapor bubble departure in forced convection boiling. *International Journal of Heat and Mass Transfer*, *36*(3), 651–662. https://doi.org/10.1016/0017-9310(93)80041-R

[5] Hidman, N., Ström, H., Sasic, S., & Sardina, G. (2022). The lift force on deformable and freely moving bubbles in linear shear flows. *Journal of Fluid Mechanics*, *952*, A34. https://doi.org/10.1017/jfm.2022.917

[6] Matsushima, H., Nishida, T., Konishi, Y., Fukunaka, Y., Ito, Y., & Kuribayashi, K. (2003). Water electrolysis under microgravity Part 1. Experimental technique. *Electrochimica Acta*, *48*(28), 4119–4125. https://doi.org/10.1016/S0013-4686(03)00579-6

[7] Akay, Ö., Bashkatov, A., Coy, E., Eckert, K., Einarsrud, K. E., Friedrich, A., Kimmel, B., Loos, S., Mutschke, G., Röntzsch, L., Symes, M. D., Yang, X., & Brinkert, K. (2022). Electrolysis in reduced gravitational environments: current research perspectives and future applications. *npj Microgravity*, *8*, 56. https://doi.org/10.1038/s41526-022-00239-y

[8] Cho, K. M., Deshmukh, P. R., & Shin, W. G. (2021). Hydrodynamic behavior of bubbles at gas-evolving electrode in ultrasonic field during water electrolysis. *Ultrasonics Sonochemistry*, *80*, 105796. https://doi.org/10.1016/j.ultsonch.2021.105796

[9] Akay, Ö., Monfort-Castillo, M., St Francis, T., and Brinkert, K., "Magnetically Induced Convection Enhances Water Electrolysis in Microgravity," *Nature Chemistry*, Vol. 17, 2025, pp. 1673–1679. https://doi.org/10.1038/s41557-025-01890-0

[10] McCrory, C. C. L., Jung, S., Ferber, I. M., Chatman, S. M., Peters, J. C., and Jaramillo, T. F., "Principles and Implementations of Electrolysis Systems for Water Splitting," *Materials Horizons*, Vol. 3, No. 4, 2016, pp. 314–446. https://doi.org/10.1039/C6MH00016A

[11] *Pingarrón, J. M., Labuda, J., Barek, J., Brett, C. M. A., Camões, M. F., Fojta, M., & Hibbert, D. B. (2020). Terminology of electrochemical methods of analysis (IUPAC Recommendations 2019). Pure and Applied Chemistry, 92(4), 641–694. https://doi.org/10.1515/pac-2018-0109*